

## Supplementary text

### Simulated lifecycle

Here we describe the simulated lifecycle, which mimics that used in previous models of evolutionary rescue in gradually changing environments (Bürger and Lynch 1995). Let  $n_i(t)$  be the number of individuals with genotype  $i \in \{aa, Aa, AA\}$  at the beginning of generation  $t$ , with  $N(t) = \sum_i n_i(t)$  the total population size. Viability selection, where genotype  $i$  survives with probability  $V_i \in [0, 1]$ , is assumed to occur before reproduction. Each surviving individual then “mothers”  $B$  offspring, each with a randomly chosen mate (possibly oneself), and each mating produces a single offspring. If there are more than  $N(0)$  offspring (we assume the population starts at carrying capacity) we randomly choose  $N(0)$  to begin the next generation.

We next describe the deterministic allele frequency dynamics. Let  $p_{j,k}(i)$  be the probability a mating between genotypes  $j$  and  $k$  produces an offspring with genotype  $i$ . The expected number of individuals of genotype  $i$  after reproduction is then

$$n_i^*(t) = \sum_{j,k} \tilde{n}_j(t) B \frac{\tilde{n}_k(t)}{\tilde{N}(t)} p_{j,k}(i), \quad (A1)$$

where  $\tilde{n}_i(t) = n_i(t)V_i$  is the expected number of individuals with genotype  $i$  and  $\tilde{N}(t) = \sum_i \tilde{n}_i(t)$  is the expected population size after viability selection. Assuming fair Mendelian transmission, the expected number of  $A$  alleles after reproduction is  $n_{Aa}^*(t) + 2n_{AA}^*(t) = W_{Aa}n_{Aa}(t) + 2W_{AA}n_{AA}(t)$ , where  $W_i = V_i B$  is referred to as the fitness of genotype  $i$ . Given that the total number of alleles after reproduction is expected to be  $2N^*(t) = 2\sum_i n_i(t)W_i = 2N(t)\bar{W}(t)$ , where  $\bar{W}(t)$  is the mean population fitness at the beginning of generation  $t$ , the expected frequency of allele  $A$  after reproduction is

$$p^*(t) = \frac{\frac{1}{2}W_{Aa}p_{Aa}(t) + W_{AA}p_{AA}(t)}{\bar{W}(t)}, \quad (A2)$$

where  $p_i(t) = n_i(t)/N(t)$  is the frequency of genotype  $i$  in generation  $t$ . Since density-dependence is random it does not change this expectation, so that the allele frequency in next generation is  $p(t+1) = p^*(t)$ . Thus the allele frequency dynamics are the same as those in a population of constant size with relative fitnesses  $W_i$  (equation 5.2.3 in Crow and Kimura 1970). Further, one can use Equation A2 to show that the genotype frequencies are expected to remain in Hardy-Weinberg proportions, allowing us to capture the dynamics of the whole system by tracking only the expected changes in the frequency of allele  $A$  and total population size (Equation 1).

### Genetic drift in the simulated lifecycle

**Probability of establishment** In our simulated lifecycle, in generation  $t$  a rare allele with a viability of  $V_i$  survives to reproduction with probability  $V_i$ , and given so, is present in  $Y + Z$  offspring, where  $Y$  is binomial with  $B$  trials and probability of success  $1/2$  (number of offspring mothered and Mendelian segregation), and  $Z$  is binomial with parameters  $BN(t)$  and  $(1/N(t))/2$  (randomly chosen as a father and Mendelian segregation). With  $\bar{V}$  the population mean viability, the expected number of offspring produced is  $N(t)B\bar{V} = N(t)\bar{W}$ . When this is less than  $N(0)$  there is no density dependence, so that all offspring survive to the next generation, while if  $N(t)\bar{W} > N(0)$  we randomly choose  $N(0)$  offspring to begin the next generation, implying each survives with probability  $N(0)/(N(t)\bar{W})$ .

From this we can calculate the mean and variance in the number of mutant alleles contributed to the next generation by a rare mutant allele in an individual with viability  $V_i$ . In the absence of density dependence (e.g., in a declining population, where  $\bar{W} < 1$ ) the expected number of copies of the allele contributed to the next generation is  $W_i = BV_i$  and the variance is  $W_i(3 + 4(B - W_i))/4 + O(1/N(t))$ . In a large population the heterozygote therefore has growth rate  $\epsilon = W_{Aa} - 1$  and variance  $v = W_{Aa}(3 + 4(B - W_{Aa}))/4$ , which we use in calculating its probability of establishment (Equation 2) for the forward-time predictions.

With density dependence (i.e., when  $N(t)\bar{W} > N(0)$ ) the expected number of copies contributed to the next generation is  $(W_i/\bar{W})(N(t)/N(0))$  and the variance is  $(W_i(3 + 4(B - W_i))/4)(N(t)/(N(0)\bar{W}))^2 + O(1/N(t))$ . When the current population size is  $N(0)$  these reduce to  $W_i/\bar{W}$  and  $W_i(3 + 4(B - W_i))/(4\bar{W}^2) + O(1/N(t))$ . Thus the backward-time growth rate of the heterozygote in a large population of mutant homozygotes at carrying capacity is  $\epsilon = 1 - W_{Aa}/W_{AA}$  and its variance is  $W_{Aa}(3 + 4(B - W_{Aa}))/4W_{AA}^2$ , which we use in calculating the probability of establishment (Equation 2) for the effective final allele frequency (Equation 3).

**Effective population size** With slow changes in population size,  $N(t-1) \approx N(t)$  and the mean number of gametes contributed to the next generation by each diploid individual in the current generation is 2. The inbreeding and variance effective population size,  $N_e(t)$ , is then roughly  $(4N(t) - 2)/(\sigma^2 + 2)$  (equation 7.6.4.3 in Crow and Kimura 1970), where  $\sigma^2$  is the variance in the number of gametes contributed to the next generation by a parent. Therefore, in a large population,  $N(t) \gg 1$ , the ratio of the effective size to the census size is roughly  $N_e(t)/N(t) \approx 4/(2 + \sigma^2)$ , where  $\sigma^2$  depends on the particular lifecycle.

In our lifecycle, in a large population with weak selection ( $W_i \approx \bar{W} \approx 1$ ) the variance is  $\sigma^2 \approx 4B - 3$  regardless of whether or not the population is at carrying capacity (File S1). We therefore use  $\sigma^2 = 4B - 3$  to calculate the effective population size,  $N_e(t)/N(t) \approx 4/(2 + \sigma^2)$  (see Event rates). Throughout we use  $B = 2$ , meaning that  $\sigma^2 \approx 5$  and  $N_e(t)/N(t) \approx 7/4$ , and thus our model imparts nearly twice as much drift as a large Wright-Fisher population (where  $\sigma^2 \approx 2$ ).

Note that drift increases with  $B$  because larger  $B$  imply that fewer individuals survive viability selection ( $V = W/B$ ) but those that do have more offspring. To keep our model close to a Wright-Fisher population we use the smallest value of  $B$  consistent with long-term population persistence,  $B > 1$ . An alternative model where the expected number of offspring upon reproduction is any positive real number, say Poisson with mean  $B$ , would allow rates of drift closer to that of a Wright-Fisher population (by setting  $B$  closer to 1).

### Simulation details

Forward-time simulations of the life-cycle described in Simulated lifecycle were performed in SLiM (version 3.3; Haller and Messer 2019) with tree-sequence recording (Haller et al. 2019).

We simulated 20 Mb chromosomes with the selected locus one of the centre bases, all other sites were neutral. We assumed a per base pair recombination rate of  $r_{bp} = 2 \times 10^{-8}$  (i.e., 2 cM/Mb; e.g., Mackay et al. 2012) and per base mutation rate at neutral loci of  $U = 6 \times 10^{-9}$  (e.g., Haag-Liautaud et al. 2007). The recombination rate between two loci  $n$  bases apart was

calculated as the probability of an odd number of crossover events assuming  $n$  independent Bernoulli trials,  $r = (1 - (1 - 2r_{bp})^n)/2 \approx (1 - e^{-2r_{bp}n})/2$  (equation 3 in [Haldane 1919](#)), i.e., no crossover interference.

A population was considered rescued (or a sweep complete) when the beneficial mutation was fixed and the population size had recovered to  $N(0)$ . Once a population was rescued we used `msprime` ([Kelleher et al. 2016](#)) to recapitate the population (simulate the neutral coalescent back in time from the start of the forward-time simulation, using Hudson's algorithm, until all sites had fully coalesced) using an effective population size of  $N_e(0) = 4N(0)/7$ .

From a random sample of chromosomes in the population at the time it was considered rescued, average pairwise diversity (Tajima's  $\pi$ ), Tajima's  $D$ , and site-frequency spectra were calculated across 100 adjacent non-overlapping windows (i.e., each of length 200 Kb  $\approx$  0.4 cM) using the `diversity()`, `Tajimas_D()`, and `allele_frequency_spectrum()` functions in `tskit` ([Kelleher et al. 2018](#)). We use a sample size of 100 chromosomes throughout. Linkage disequilibrium was calculated by first identifying the segregating mutation closest to each window's midpoint and then using `tskit.LdCalculator().r2()` to calculate disequilibrium between it and the segregating mutation closest to a recombination distance of  $r = 0.001$  away.

For comparison we also run simulations with a constant expected population size by setting  $d = 0$ . In this case the ancestral genotype  $aa$  has an absolute fitness of 1, meaning that any realized population size trajectory will be a random walk with an upper boundary at  $N(0)$  so that extinction is assured in the long-term. However, with the parameter values used here (relatively large initial population size and fast onset of the selective sweeps), populations decline only slightly before remaining constant at the carrying capacity once the sweep has started in earnest (since the mutants have fitnesses  $\geq 1$ ). We chose to use this setup as the constant population size comparison (rather than, say, a Wright-Fisher population) because it allows us to keep the same variance in gamete numbers (affecting the probability of establishment and the rate of coalescence; see [Genetic drift in the simulated lifecycle](#)) as well as the same census population size (affecting the initial and effective allele frequencies) as in the case of rescue.

### Deriving the structured coalescent

Let the allele frequency and population size  $\tau$  generations before the present be  $p'(\tau)$  and  $N'(\tau)$ . Following [Pennings and Hermisson \(2006a\)](#), we artificially subdivide the time within a generation to be able to identify any period between two successive events in our lifecycle (Figure A1). We now go about deriving the probabilities in the structured coalescent (Equation 6).

**Migration** The number of migrant alleles that arrive each generation is Poisson with mean  $m$ . Given that there are  $2N'(\tau - 1)p'(\tau - 1)$  beneficial alleles in the next generation, the probability that any one is a new migrant is therefore  $P = m/[2N'(\tau - 1)p'(\tau - 1)] \approx m/[2N'(\tau)p'(\tau)]$ , where the approximation assumes the number of beneficial alleles changes little from one generation to the next. The probability that at least one of  $k$  beneficial alleles is a migrant is  $1 - (1 - P)^k$ , which, with rare migration, is approximately

$$p_{\text{mig}}(k, \tau) = k \frac{m}{2N'(\tau)p'(\tau)}. \quad (\text{A3})$$

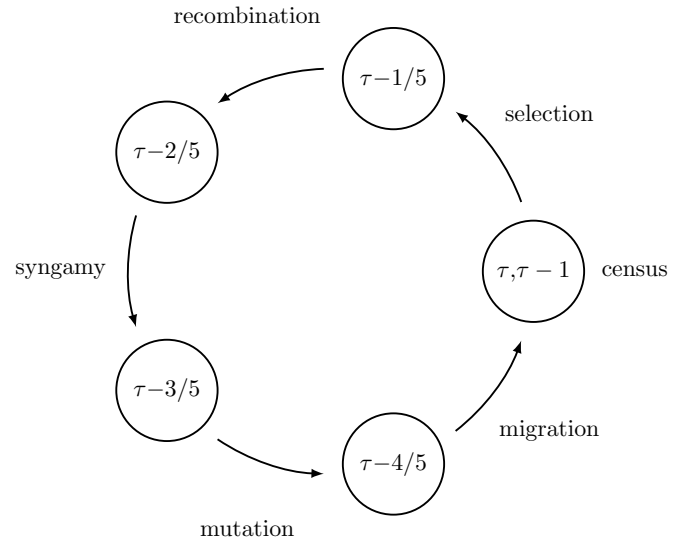


**Figure A1** Life-cycle and time notation. The arrows indicate the forward-time direction and the numbers indicate the time before fixation (i.e., starting in generation  $\tau$  and moving forward in time through  $\tau - 1/5$ ,  $\tau - 2/5$ , ... we arrive at generation  $\tau - 1$ , one generation closer to fixation).

For a given probability of being replaced by a migrant allele, the rate of migration in a diploid model is half that of the haploid model (equation 15 in [Pennings and Hermisson 2006a](#), replacing  $M$  with  $m$ ) as there are twice as many resident alleles.

**Mutation** The number of beneficial alleles after mutation,  $2N'(\tau - 4/5)p'(\tau - 4/5)$ , is the number before mutation plus the number of new mutants

$$2N'(\tau - 4/5)p'(\tau - 4/5) = 2N'(\tau - 3/5)p'(\tau - 3/5) + u2N'(\tau - 3/5)[1 - p'(\tau - 3/5)]. \quad (\text{A4})$$

Because the population size does not change during mutation,  $N'(\tau - 4/5) = N'(\tau - 3/5)$ , the frequency of beneficial alleles after mutation is simply

$$p'(\tau - 4/5) = p'(\tau - 3/5) + u[1 - p'(\tau - 3/5)]. \quad (\text{A5})$$

The probability a beneficial allele is a new mutant is therefore  $u[1 - p'(\tau - 3/5)]/p'(\tau - 4/5)$ , which, using Equation A5, is equivalent to

$$P = \frac{u[1 - p'(\tau - 4/5)]}{(1 - u)p'(\tau - 4/5)}. \quad (\text{A6})$$

The probability that at least one of  $k$  beneficial alleles is a new mutant is  $1 - (1 - P)^k$ , which, when mutation is rare, is approximately  $ku[1 - p'(\tau - 4/5)]/p'(\tau - 4/5)$ . With little change in allele frequency from one generation to the next this is approximately

$$p_{\text{mut}}(k, \tau) = ku \frac{1 - p'(\tau)}{p'(\tau)}. \quad (\text{A7})$$

This is equivalent to the haploid result (e.g., equation 5 in [Pennings and Hermisson 2006a](#)) as both the mutation rate and number of alleles are multiplied by the ploidy level, which cancels.

**Coalescence** Considering  $k$  beneficial alleles at the time of census, and ignoring any migration or mutation, the probability of at least one coalescence event is then

$$\binom{k}{2} \frac{1}{2N'_e(\tau - 2/5)p'(\tau - 2/5)}, \quad (\text{A8})$$

where  $N'_e(\tau - 2/5)$  is the effective population size at the time of syngamy. When allele frequency and effective population size changes little from one generation to the next this is roughly

$$p_{\text{coal}}(k, \tau) = \binom{k}{2} \frac{1}{2N'_e(\tau)p'(\tau)}. \quad (\text{A9})$$

This is half the rate observed in a haploid model with the same population size (equation 5 in Pennings and Hermisson 2006a) as there are twice as many alleles in a diploid population.

**Recombination** Consider a neutral locus at recombination distance  $r$  from the selected site. Assuming weak selection such that the survivors of viability selection remain in Hardy-Weinberg proportions, the number of alleles linked to the beneficial allele after recombination is

$$\begin{aligned} & 2N'(\tau - 2/5)p'(\tau - 2/5) \\ &= 2N'(\tau - 1/5)p'(\tau - 1/5) \\ & [p'(\tau - 1/5) + [1 - p'(\tau - 1/5)](1 - r)] \\ &+ N'(\tau - 1/5)[1 - p'(\tau - 1/5)]p'(\tau - 1/5)r. \end{aligned} \quad (\text{A10})$$

The first term on the right hand side is the number of alleles linked to the beneficial allele before recombination multiplied by the probability of being in a beneficial homozygote plus the probability of being in a heterozygote but not recombining. The second term on the right hand side is the number of alleles not linked to the beneficial allele before recombination times the probability of being in a heterozygote and recombining onto the beneficial background. The probability an allele on the beneficial background after recombination was not there before is then

$$P = \frac{2N'(\tau - 1/5)[1 - p'(\tau - 1/5)]p'(\tau - 1/5)r}{2N'(\tau - 2/5)p'(\tau - 2/5)}, \quad (\text{A11})$$

which, because recombination does not change allele frequency or population size, is

$$\begin{aligned} P &= \frac{2N'(\tau - 1/5)[1 - p'(\tau - 1/5)]p'(\tau - 1/5)r}{2N'(\tau - 1/5)p'(\tau - 1/5)} \\ &= [1 - p'(\tau - 1/5)]r. \end{aligned} \quad (\text{A12})$$

The probability at least one of  $k$  alleles on the beneficial background recombines off is  $1 - (1 - P)^k$ , which, when recombination is rare, is approximately  $kr[1 - p'(\tau - 1/5)]$ . Assuming allele frequency changes little through one bout of selection this is  $kr[1 - p'(\tau)]$ . Finally, assuming migration, mutation, and coalescence are rare, the probability that none of  $k$  beneficial alleles migrate or mutate times the probability none coalesce times the probability at least one of the  $k$  linked alleles recombines off is roughly (table 1 in Hudson and Kaplan 1988)

$$p_{\text{rec}}(k, \tau) = kr[1 - p'(\tau)]. \quad (\text{A13})$$

## A simultaneous, but independent, bottleneck and sweep from SGV

In [Rescue from standing genetic variation \(SGV\)](#) we have compared the genetic signatures of rescue to those from sweeps in populations of constant size. Two of key differences we have identified, lower absolute diversity and positive Tajima's  $D$  at unlinked sites under rescue, arise simply because of the population bottleneck. This suggests that it will be yet harder to distinguish rescue from a sweep that occurs during a bottleneck, where the sweep and bottleneck are coincident but independent. Taking this argument to its logical limit, if the population size dynamics during an externally forced bottleneck are exactly like those expected under rescue, then the expected genetic signatures will be identical. As a middle-ground, we can compare an instance of rescue that has an expected effective population size of  $N_e$  during its sweep to a population that is bottlenecked to a constant effective population size  $N_e$  during its sweep (let's call the latter the 'coincident' scenario). Then, under the same allele frequency dynamics (which will not be exactly true as population size and decline rate affect the effective initial and final allele frequencies), both populations would have similar genome-wide diversity and Tajima's  $D$  values.

In File S1 we show that coincident scenario produces patterns of relative diversity at the selected site like sweeps in populations of constant size (i.e., like the red curve at 0cM in Figure ??), meaning that rescue causes deeper dips in diversity than a coincident sweep and bottleneck. This is because the coincident scenario assumes smaller population sizes at the beginning and end of the sweep, causing higher effective initial frequencies and lower effective final frequencies, which shortens the length of the sweep and thus increases the probability that no events occur in the history of the sample during the sweep,  $P_0(k, t_f)$ . These shorter sweeps also mean that the coincident scenario leaves less time for coalescence on the ancestral background and thus produces higher genome-wide absolute diversity than populations that have been rescued. In contrast, rescue and the coincident scenario similarly slow the recovery of relative diversity as we move away from the selected site, causing their dips in diversity to have similar width (i.e. like the blue curve in Figure ??). This is because both scenarios increase rates of coalescence early in the sweep, preventing recombination off and thus lowering  $P_{\text{off}}(k, t_f)$ . The shape of Tajima's  $D$  values across the genome are much the same in the coincident scenario as they are after a sweep in a population of constant size (i.e., like the red curves in Figure ??), just shifted up so that the background levels closely match those under rescue (i.e., they have intercepts like the blue curves in Figure ??). In summary: for a given strength of selection and effective population size during a sweep, the dynamics of rescue produce 1) deeper dips in diversity, 2) lower absolute diversity genome-wide, and 3) a greater range of Tajima's  $D$  values. These differences arise because the lower population sizes at the beginning and end of the coincident scenario cause faster establishment and fixation, leading to shorter sweeps.

To explore whether there is additional signal to be gained from the different timings of coalescence and recombination in the coincident and rescue scenarios we have also looked at the full site frequency spectra arising from simulations (of which pairwise diversity and Tajima's  $D$  are summaries; Wakeley 2009, p. 116). Figure A2 shows the site frequency spectra at three recombination distances for a case where relative diversity and Tajima's  $D$  values are very similar in the two scenarios ( $s = 0.2$ ,  $\kappa = 10$ ; see File S1). Far from the selected site the entire spectra



are very similar in the two scenarios, both documenting a recent short drop in population size (a deficiency of rare alleles, as indicated by positive genome-wide Tajima's  $D$ ). As we move towards the selected site the patterns diverge slightly, the harder sweep during rescue now causing a larger deficit of intermediate frequency alleles and a larger excess of high frequency alleles (as indicated by a slightly more negative Tajima's  $D$  at the shoulders of the selected site). At selected site the spectra are again very similar, although with more noise as there are less polymorphic sites. Thus the strongest signal of rescue vs. a bottlenecked sweep seems to be provided at moderately linked sites, where the relative timings and strengths of coalescence and recombination have the most impact. For instance, the timing and probability of coalescence at 1cM is nearly identical in rescue vs. the coincident scenario here, but the probability of recombination is slightly reduced and tends to occur slightly later under rescue. This reduction in recombination is predicted to create phylogenies that are more star-like, which may explain much of the greater deficit of intermediate frequency mutations. The fact that recombination is also delayed and thus overlaps more with coalescence, in rescue relative to the coincident scenario, may help explain the perhaps flatter spectrum across low to high frequency mutations near the selected site, as the overlap creates more variance in the number of coalescence events that occur prior to the lineage recombining off the sweep (similar to the effect of recurrent mutation; Pennings and Hermisson 2006b). Note that if we instead compared site frequency spectra in windows with similar absolute genetic diversity (as in figure 6 of Kim and Gulisija 2010), differences between the three scenarios would be more apparent. Thus a combination of summary statistics may help differentiate rescue from a simultaneous, but independent, bottleneck and sweep.

Site frequency spectra (and summaries of them) are characteristics of individual loci. As a final potential signature of rescue vs. the coincident scenario we look at linkage disequilibrium, which captures correlations in the pairwise coalescence times between two loci (Wakeley 2009, p. 236). Figure A3 shows linkage disequilibrium between neutral loci that are a recombination distance of  $r = 0.001$  apart, as a function of their distance from the selected site. As we can see, the sweep causes elevated linkage disequilibrium near the selected site, as expected for sites that were segregating before the sweep (Kim and Nielsen 2004; McVean 2007). Meanwhile population bottlenecks tend to increase linkage disequilibrium genome wide, as expected given that bottlenecks decrease mean coalescence times more than they decrease the variance (McVean 2002). The differences in linkage disequilibrium patterns between the rescue and coincident scenario are much greater than the differences observed in relative diversity, Tajima's  $D$ , or the full site frequency spectrum. The differences in linkage disequilibrium do, however, largely mirror those observed in absolute diversity (see File S1), which can largely be explained by the shorter sweeps, and thus less coalescence, in the coincident scenario.

#### **Population dynamics and the coalescent under rescue by migration**

**Effective initial allele frequency and the backward-time dynamics** Dividing the (truncated) exponential waiting time distribution for the first successful migrant allele by the probability of rescue gives the waiting time distribution conditioned on rescue. Following the same approach as above (see ??), the effective

initial frequency of the beneficial allele given rescue is then

$$p_{0|\text{rescue}}^{\text{MIG}} = \frac{1}{2N(0)} \frac{1}{P_{\text{est}}} \frac{2m \left(1 - (1 - p_{\text{rescue}}^{\text{MIG}})N(0)^{-P_{\text{est}}/(2d)}\right)}{(1 + 2m)p_{\text{rescue}}^{\text{MIG}}}. \quad (\text{A14})$$

When the migration rate is small this last factor is nearly independent of  $m$  (analogous to the mutation case). As in the case of *de novo* mutation, to characterize the backward-time dynamics in a population of constant size we do not need to know when the sweep begins, just the effective initial frequency at this time,  $1/(2N(0)P_{\text{est}})$ .

Figure A4 compares our analytical approximations (Equations 5 and A14) against individual-based simulations. We see the predictions do fairly well for larger values of  $m$ , but can fair quite poorly with small  $m$ . In the latter case the first successful migrant allele sometimes arrives when the population is so small that the beneficial allele increases in frequency much faster than the deterministic expectation. Here we enter a different regime, which we do not attempt to approximate.

**The structured coalescent** Figure A5 shows the timing of migration relative to recombination and coalescence (Equation 7). As with rescue from standing genetic variance or mutation (Figures ?? and ??), the bottleneck increases the overall coalescence rate and shifts its timing closer to fixation, overlapping more with recombination. Migration scales with coalescence (Equation 6) and is thus similarly increased and shifted. When migration rates are small enough that the migrant allele tends to fix when the population is very small the simulations show an initial spike in expected coalescence, which is expected to greatly reduce diversity.

**Genetic signatures at linked neutral loci** The genetic signatures at linked neutral loci produced by a sweep that arises from migration depends on the history of the metapopulation, e.g., how and when the sweeps occurred in each patch and the historical migration rates between them. We therefore omit an exploration of the signatures produced in this scenario, which deserves a full and careful treatment on its own. Previous work has explored some potential signatures of migrant sweeps in populations of constant size. For example, if the historic migration rate between the migrant and focal population is low then we should expect few migrant alleles away from the selected site. Then, under low contemporary migration rates we expect a relatively hard sweep and the so-called "volcano" pattern of genetic diversity (Setter et al. 2019), where diversity is maximized at an intermediate distance from the selected site due to a more balanced presence of both migrant and non-migrant alleles.

#### **Literature Cited**

- Bürger, R. and M. Lynch, 1995 Evolution and extinction in a changing environment: a quantitative-genetic analysis. *Evolution* 49: 151–163.
- Crow, J. F. and M. Kimura, 1970 *An introduction to population genetics theory*. Harper & Row.
- Haag-Liautard, C., M. Dorris, X. Maside, S. Macaskill, D. L. Halligan, et al., 2007 Direct estimation of per nucleotide and genomic deleterious mutation rates in *Drosophila*. *Nature* 445: 82.
- Haldane, J. B. S., 1919 The combination of linkage values, and the calculation of distances between the loci of linked factors. *Journal of Genetics* 8: 299–309.

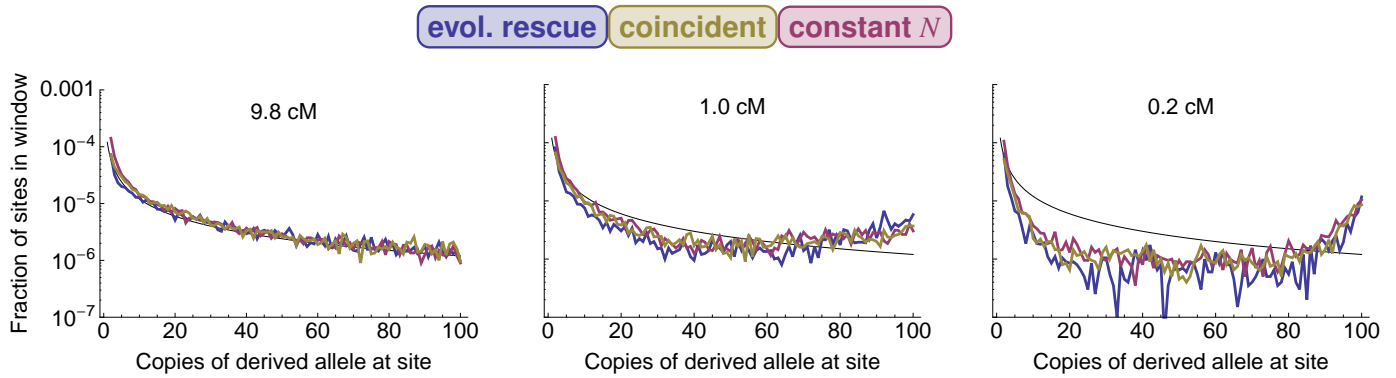


**Figure A2** Site frequency spectra at three distances from the selected site after a selective sweep from standing genetic variation in evolutionary rescue (blue;  $N(0) = 10^4$ ,  $d = 0.05$ ), in a bottlenecked population with short-term effective population size similar to that in rescue (yellow;  $N(0) = 2945$ ,  $d = 0$ ), or in a population of constant size (red;  $N(0) = 10^4$ ,  $d = 0$ ). Blue, yellow, and red curves are mean values from 100 replicate simulations. The black curve is the neutral expectation,  $4N_eU/x$ , where  $N_e$  is the long-term effective population size (here  $10^4 \times 4/7$ ) and  $x$  is the number of copies of the derived allele. Parameters:  $s = 0.2$ ,  $\kappa = 10$ .

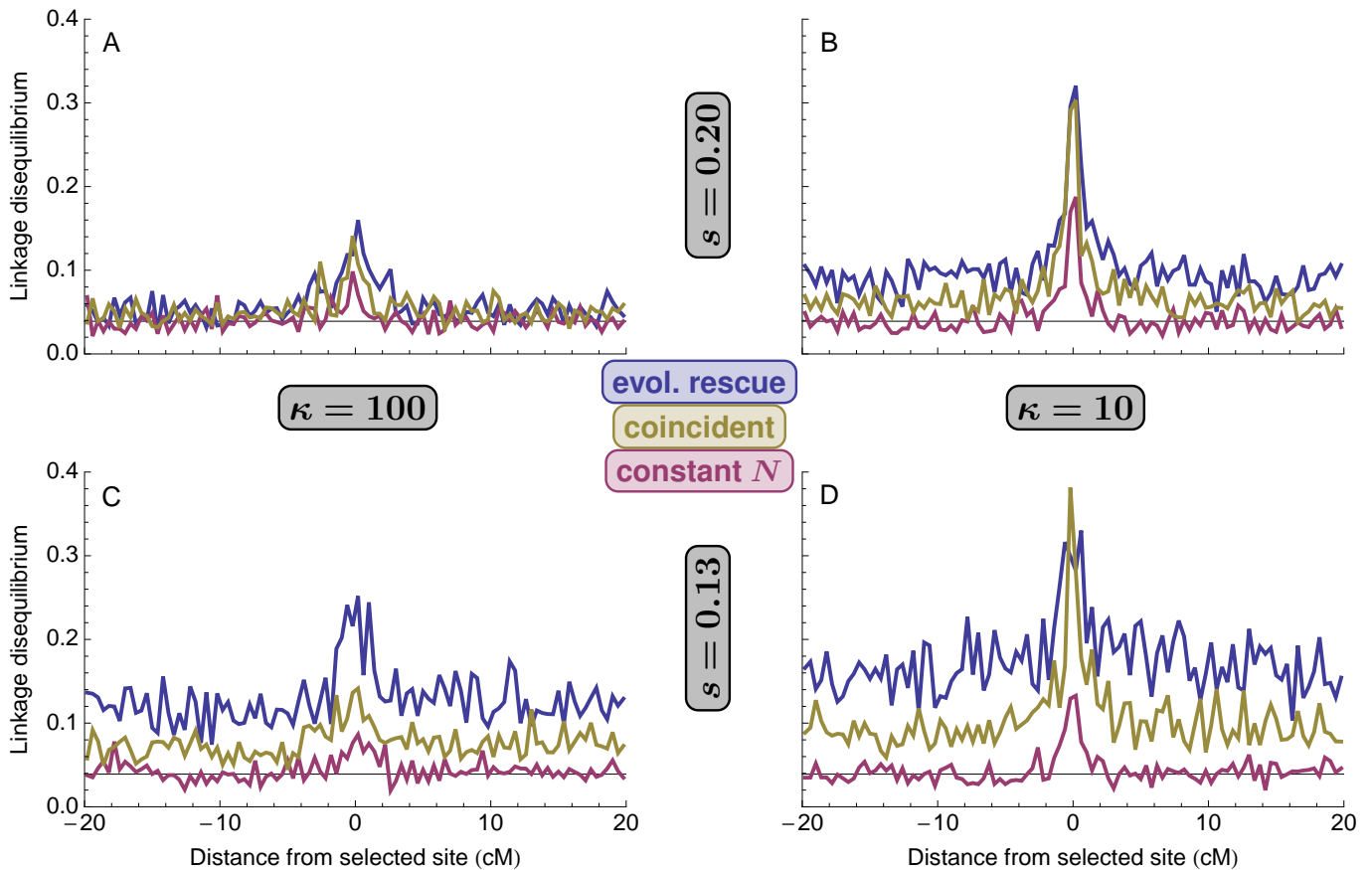


**Figure A3** Linkage disequilibrium,  $r^2$ , between neutral loci that are recombination distance 0.001 apart after a selective sweep from standing genetic variation in evolutionary rescue (blue;  $N(0) = 10^4$ ,  $d = 0.05$ ), in a bottlenecked population with short-term effective population size similar to that in rescue (yellow;  $N(0) = 2945$ ,  $d = 0$ ), or in a population of constant size (red;  $N(0) = 10^4$ ,  $d = 0$ ). The black line is the neutral expectation (equation 7.31 in Wakeley 2009).

Haller, B. C., J. Galloway, J. Kelleher, P. W. Messer, and P. L. Ralph, 2019 Tree-sequence recording in SLiM opens new horizons for forward-time simulation of whole genomes. *Molecular Ecology Resources* **19**: 552–566.

Haller, B. C. and P. W. Messer, 2019 SLiM 3: forward genetic sim-

ulations beyond the Wright–Fisher model. *Molecular Biology and Evolution* **36**: 632–637.

Hudson, R. R. and N. L. Kaplan, 1988 The coalescent process in models with selection and recombination. *Genetics* **120**: 831–840.

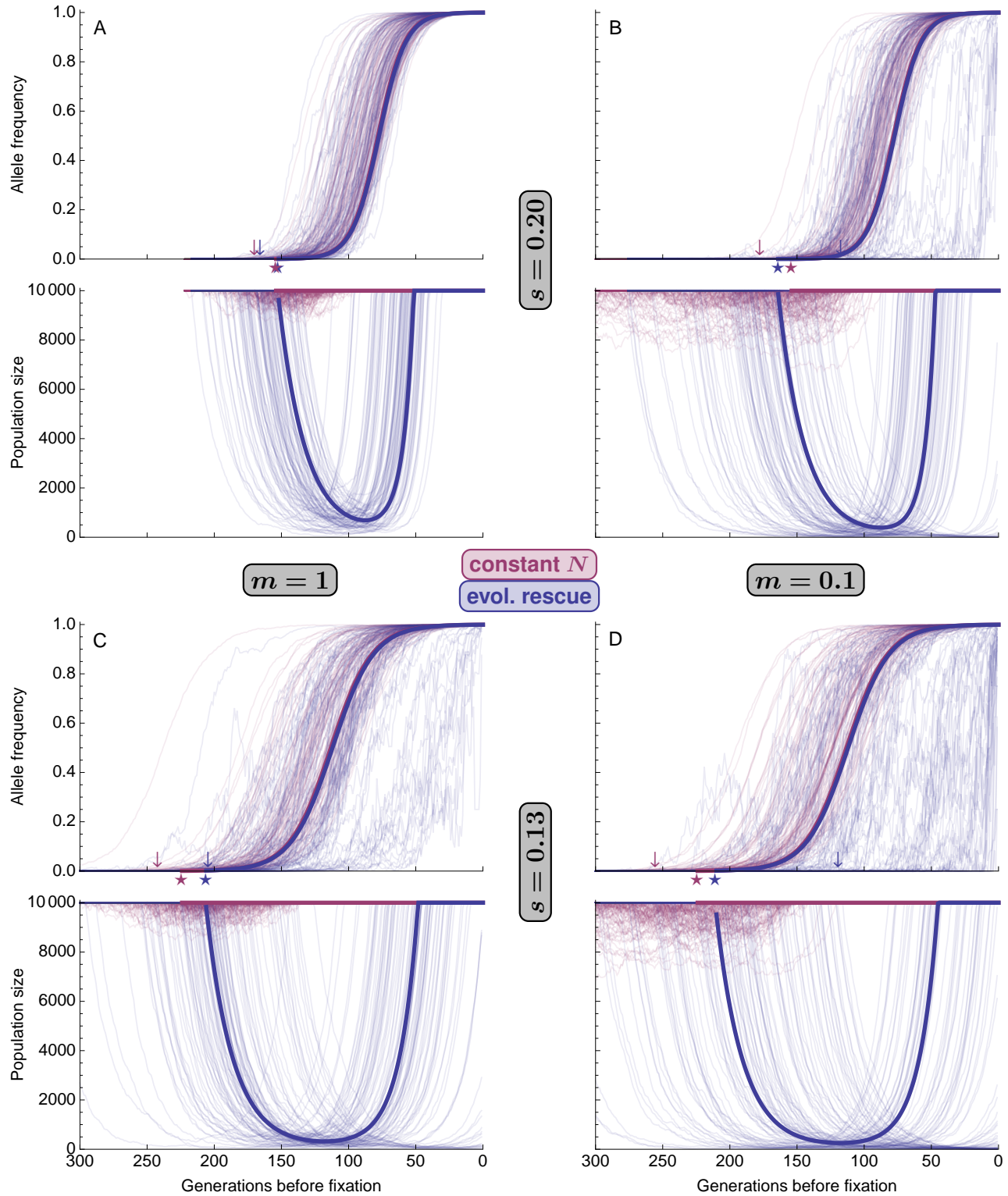


**Figure A4** Allele frequency and population size during a selective sweep from migration in evolutionary rescue (blue;  $d = 0.05$ ) or in a population of roughly constant size (red;  $d = 0$ ). The thick solid curves are analytic approximations (Equation 5), using  $p_0 = p_{0|rescue}^{MIG}$  (Equation A14) as the initial frequency and  $p_f$  (Equation 3) as the final allele frequency. The thin curves are 100 replicate simulations where a sweep (and population recovery) was observed. The stars show the predicted time to fixation (Equation 4). The arrows show the mean time to fixation observed in simulations.

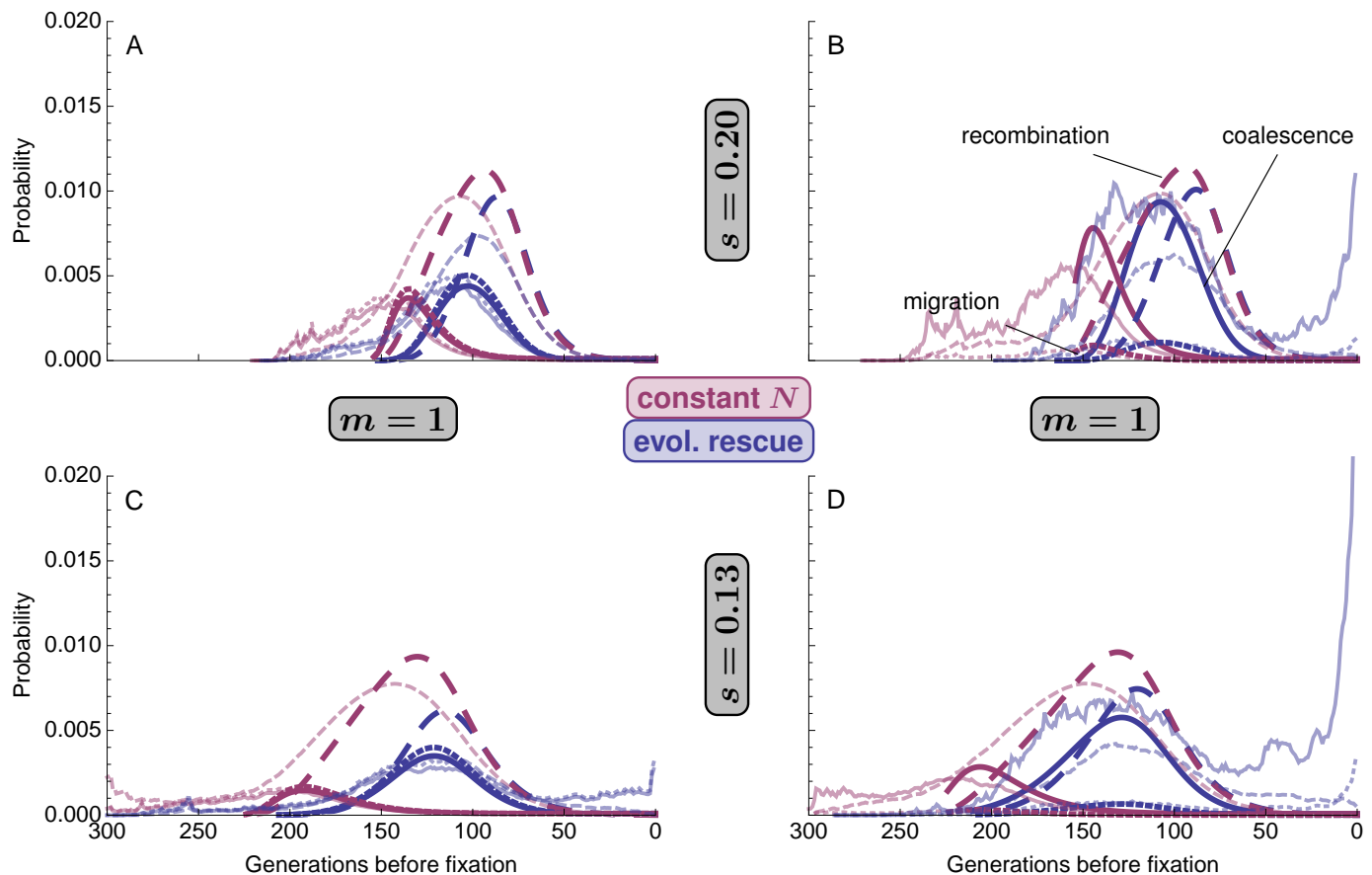


**Figure A5** The timing of events in the structured coalescent (Equation 7) for a sample of size  $k = 2$  at a linked neutral locus ( $r = 0.01$ ) during a selective sweep from migration in evolutionary rescue (blue;  $d = 0.05$ ) or in a population of roughly constant size (red;  $d = 0$ ). Thicker opaque curves use the analytic expressions for allele frequency and population size (Equation 5) while the thinner transparent curves show the mean probabilities given the observed allele frequency and population size dynamics in 100 replicate simulations (these become more variable in the past as less replicates remain polymorphic).

Kelleher, J., A. M. Etheridge, and G. McVean, 2016 Efficient coalescent simulation and genealogical analysis for large sample sizes. *PLoS Computational Biology* **12**: 1–22.

Kelleher, J., K. R. Thornton, J. Ashander, and P. L. Ralph, 2018 Efficient pedigree recording for fast population genetics simulation. *PLoS Computational Biology* **14**: e1006581.

Kim, Y. and D. Gulisija, 2010 Signatures of recent directional selection under different models of population expansion during colonization of new selective environments. *Genetics* **184**: 571–585.

Kim, Y. and R. Nielsen, 2004 Linkage disequilibrium as a signature of selective sweeps. *Genetics* **167**: 1513–1524.

Mackay, T. F., S. Richards, E. A. Stone, A. Barbadilla, J. F. Ayroles, *et al.*, 2012 The *Drosophila melanogaster* genetic reference panel. *Nature* **482**: 173.

McVean, G., 2007 The structure of linkage disequilibrium around a selective sweep. *Genetics* **175**: 1395–1406.

McVean, G. A., 2002 A genealogical interpretation of linkage disequilibrium. *Genetics* **162**: 987–991.

Pennings, P. S. and J. Hermisson, 2006a Soft sweeps II: molecular population genetics of adaptation from recurrent mutation or migration. *Molecular Biology and Evolution* **23**: 1076–1084.

Pennings, P. S. and J. Hermisson, 2006b Soft sweeps III: the signature of positive selection from recurrent mutation. *PLoS*

*Genetics* **2**: e186.

Setter, D., S. Mousset, X. Cheng, R. Nielsen, M. DeGiorgio, *et al.*, 2019 VolcanoFinder: genomic scans for adaptive introgression. *bioRxiv* **697987**.

Wakeley, J., 2009 *Coalescent theory*. Roberts & Company.